Carbohydrate Polymers 105 (2014) 184–192

Contents lists available at ScienceDirect

Carbohydrate Polymers

journal homepage: www.elsevier.com/locate/carbpol

Superporous thermo-responsive hydrogels by combination of cellulose fibers and aligned micropores

Kantappa S. Halake, Jonghwi Lee*

Department of Chemical Engineering and Material Science, Chung-Ang University, Seoul 156-756, South Korea

ARTICLE INFO

Article history:
Received 29 September 2013
Received in revised form 7 January 2014
Accepted 8 January 2014
Available online 20 January 2014

Keywords:
Microfibrillated cellulose
Directional freezing
Composite
Superporous hydrogel
Responsive hydrogel
Micropore
Superabsorbent

ABSTRACT

In the area of artificial hydrogels, simultaneous engineering of the volume transition characteristics and mechanical properties of stimuli-responsive hydrogels is an important subject. By unrestricted architecting of hierarchical structures, natural hydrogels are able to provide a wide range of swelling and mechanical properties, beyond the limits of artificial hydrogels. Herein, a combination of nanostructures and microstructures was developed to construct superporous hydrogels. Fibers of microfibrillated cellulose (MFC), an eco-friendly reinforcing material, were used as nanostructures, aligned micropores were used as microstructures, and *in situ* photopolymerization was used to immobilize the two structures together within the gel networks of poly(N-isopropyl acrylamide) (PNIPAm). The introduction of MFC distinctly enhanced volume transition, mainly by decreasing the swelling ratios above the transition. The introduction of directional micropores increased the swelling ratio below the transition and decreased the swelling ratio above the transition, thereby also enhancing the volume transition. Additionally, the formation of aligned micropores achieved fast water infiltration, which is beneficial for superabsorbent applications. The introduction of aligned micropores reduced the elastic modulus, but this could partially be compensated for by reinforcement with MFC. This combination of crystalline nanofibers and aligned micropores has great potential for the development of stimuli-responsive superporous hydrogels outperforming current artificial hydrogels.

1. Introduction

Hydrogels are typically three-dimensional networks of hydrophilic molecular chains; they exhibit unique viscoelastic behaviors that can be stimuli-responsive. The most widely studied temperature-responsive hydrogel is poly(N-isopropylacrylamide) (PNIPAm), which has a lower critical solution temperature (LCST) of *ca.* 32 °C (Hou et al., 2008; Li, Guo, Chang, & Yang, 2012). Below the LCST, it is hydrophilic; above the LCST, its chain conformation changes to become hydrophobic. This transition causes water to be expelled, leading to a dramatic reduction in volume (JagadeeshBabu, Suresh Kumar, & Maheswari, 2011), a behavior that has been explained by hydrophobic interaction and the temperature dependence of the interaction parameter (Cho, Lee, & Cho, 2003). Because of their interesting physicochemical properties, synthetic hydrogels have many applications in various fields such as superabsorbent materials, pharmaceutics, food chemistry, medicine, agriculture, and biotechnology (Bajpai, Shukla, Bhanu, & Kankane, 2008).

For many applications, to be useful, materials must combine high swelling (*i.e.*, high volume change) with good mechanical properties. Many natural hydrogels exemplify this combination, such as actin, which forms filament structures rather than a simple random network (Breedveld, Nowak, Sato, Deming, & Pine, 2004). In many cases, artificial hydrogels have failed to surpass the performance of natural hydrogels, because the properties of both types are largely confined by what the rubber elasticity theory predicts; that is to say, a large swelling ratio is generally accompanied by poor mechanical properties (Bhattacharyya, Guillot, Dabboue, Tranchant, & Salvetat, 2008; Zhou & Wu, 2011). To overcome this limitation, hydrogels have been engineered by architecting unique molecular chain structures, nanostructures, or microstructures. Several studies have been reported to improve the modulus and strength of hydrogels by incorporating organic or inorganic fillers such as carbon nanotubes and sodium montmorillonite layered silicates (Bhattacharyya et al., 2008; Xia, Yih, D'Souza, & Hu, 2003; Yildirim, Yin, Nair, & Sun, 2008; Zhou & Wu, 2011). Composite hydrogels have showed enhanced elastic modulus, but without notable improvement in swelling ratio (Wang et al., 2012; Xia et al., 2003).

Crystalline cellulose, an abundantly available natural polysaccharide, is a renewable material suitable for the reinforcement of composites. Pure celluloses cannot be isolated easily from plants,

* Corresponding author. Tel.: +82 2 816 5269; fax: +82 2 824 3495.
E-mail addresses: jong@cau.ac.kr, leexx303@gmail.com (J. Lee).

0144-8617/$ – see front matter © 2014 Elsevier Ltd. All rights reserved.
http://dx.doi.org/10.1016/j.carbpol.2014.01.025

due to strong interactions with a number of associated macromolecules such as lignin, hemicellulose, and tannin (Chen et al., 2011). However, pure crystalline celluloses can be purified from bacteria, algae, and tunicates; the celluloses initially contain both highly ordered (crystalline) and less ordered (amorphous) phases (Chen et al., 2011; Martínez-Sanz, Lopez-Rubio, & Lagaron, 2011; Tischer, Sierakowski, & Tischer, 2010). Sulfuric acid hydrolysis is one of the routes to remove the disordered phases and obtain highly crystalline celluloses (Correa, Teixeira, Pessan, & Mattoso, 2010; Tischer et al., 2010). Purified microfibrillated celluloses (MFCs) 5–20 nm in diameter have been widely investigated for use as dry composites, but seldom for reinforcing hydrogels because effective load transfer is unlikely from the matrix to the MFCs. Instead, interpenetrating networks or double networks have been developed intensively (Gong, Katsuyama, Kurokawa, & Osada, 2003). However, because decreased volume transition could ensure effective load transfer, simple embedding MFC with poor load transfer could be beneficial for enhanced volume transition. Furthermore, a combination of two different structures at different scales, which mimics the hierarchical structures of natural hydrogels (Lazarides, 1976), could offer a novel strategy to engineer the properties of hydrogels outside what conventional hydrogels can offer.

Herein, MFC was used as a nanostructure for reinforcement, offering plenty of hydrogen bonding sites for 'flexible' load transfer, and well-aligned cylindrical micropores were used as microstructures to tailor swelling properties. The hypothesis was investigated that a hierarchical combination of MFC and cylindrical micropores can widen the property windows of artificial hydrogels. Cylindrical micropores were introduced and aligned by directional melt crystallization (freezing) of water along a temperature gradient. The frozen water acted as a porogen; that is, it produced porous structures. The unidirectional freezing method has been exploited for preparing various aligned porous materials, including organic, inorganic, and composite materials for bioengineering, drug delivery, catalyst supports, and separation (Nishihara et al., 2006). Recently, a combined method of directional freezing and UV-induced polymerization in a frozen state successfully fabricated anisotropic microstructures (Barrow & Zhang, 2013; Chen, Zhu, Qi, He, & Wang, 2012), which seems to be a proper method to immobilize MFC in a hydrogel matrix while simultaneously forming aligned micropores.

2. Experimental

2.1. Materials

N-isopropyl acrylamide (NIPAm) from Sigma–Aldrich (St. Louis, MO, USA) was purified by dissolution and recrystallization in n-hexane (Convertine et al., 2006). Methylenebisacrylamide (MBA) and concentrated sulfuric acid (H_2SO_4) were used as received from Sigma–Aldrich. Irgacure 2959 (initiator) was purchased from Tokyo Chemical Industry (Tokyo, Japan). Distilled water, ethanol, and n-hexane were purchased from Duksan Chemicals (Ansan, South Korea). Kombucha was purchased from a local manufacturer (Kombucha Co., ShiHung, KyungKi, Korea); tea bags (Lipton) and food-grade sugar were purchased from a local market.

2.2. Preparation of MFC

A cellulose-producing bacterium was first isolated from commercially available kombucha tea, and a culture medium was prepared by adding a tea bag and 3 g of sugar to 100 mL of warm distilled water. Kombucha precursor of 1 mL was then inoculated into the culture medium in a 1000 mL beaker and incubated at 25 °C without agitation.

A 500 g wet mat of bacterial cellulose was cut into small pieces and washed thoroughly with water to remove the odors and color of the growth medium. The mat pieces were heated at 100 °C for 3 × 25 min in 500 mL of 10% (w/v) NaOH, and then finally washed in distilled water at RT until neutral pH was reached. The pieces were then compressed into thin sheets, squeezing out as much water as possible, and the pieces were hydrolyzed for 3 days at 30 °C using 500 mL of 50% (v/v) H_2SO_4. The hydrolysis reaction was quenched by adding 500 mL of distilled water. The dispersion was isothermally centrifuged (Mega 17R+, Hanil Centrifuge, Inchon, Korea) at 15 °C and 12,000 rpm for 25 min, followed by washing with distilled water and a second centrifugation using the same conditions. The cellulose was thereby collected at the bottom of the centrifuge tube; the acidic supernatant was discarded. To remove the excess of sulfuric acid, the cellulose residue was dialyzed in distilled water until neutral pH was reached. The water was discarded, 500 mL of acetone was added, and the tube was centrifuged using the same conditions described above. MFC was obtained as a white powder by drying in a hood overnight.

2.3. Preparation of PNIPAm and PNIPAm/MFC composite hydrogels

To prepare PNIPAm hydrogels (designated as P), NIPAm monomer (4.42 mmol), MBA crosslinker (0.032 mmol), and initiator (0.045 mmol) were dissolved in 3.5 mL of distilled water and stirred under nitrogen atmosphere for 15 min (Singh, Kuckling, Choudhary, Adler, & Koul, 2006). An appropriate amount of monomer solution (0.9 mL) was transferred into a silicone/glass mold (5 mm thick). The mold was kept in a UV chamber (27 cm × 37 cm, 365 nm) at 5 °C. After 1 h of UV illumination, the hydrogels were soaked in 1 L of distilled water for 3 days, with daily exchange of fresh water to remove unreacted impurities.

To prepare MFC/PNIPAm hydrogels (PM), a 5 wt% MFC aq. dispersion was first prepared with magnetic stirring overnight. After ultrasonication for 5 min, appropriate amounts of monomer, crosslinker, and initiator were added for the same hydrogel composition, and the same crosslinking step described above was applied. For the preparation of PNIPAm or composite hydrogels having directional micropores (PD or PMD), the solution-filled mold was directionally frozen on top of a liquid nitrogen reservoir for 10 min and then the crosslinking step described above was applied (Fig. 2). Details on the directional freezing methods are available elsewhere (Lee & Lee, 2013).

2.4. Characterization

The temperature dependence of the equilibrium swelling ratio (SR) was studied gravimetrically over the 20–50 °C range with 3 °C increments. The hydrogel samples were immersed in distilled water for 4 hr at each temperature. Each sample was blotted with moistened filter paper to remove excess water and then weighed (W_s). Five samples of each hydrogel were prepared, and the standard deviation over the 5 corresponding weight measurements was calculated. The dry weights of samples (W_d) were obtained after freeze-drying (EYELA FDU 2200, Tokyo, Japan) followed by vacuum drying at 50 °C for 24 h. SR was defined using the following equation: $SR\,(\%) = (W_s - W_d)/W_d \times 100$.

The CP/MAS ^{13}C NMR spectra of MFC fibers were collected with a VNMRS 400 spectrometer (Varian, Palo Alto, CA, USA) operating at a frequency of 400 MHz. UV–vis absorption spectra were obtained using a spectrophotometer (JASCO V-670 spectrophotometer, Japan), using samples of 1.8 mm thickness and using distilled water as a reference. To retain sample morphology

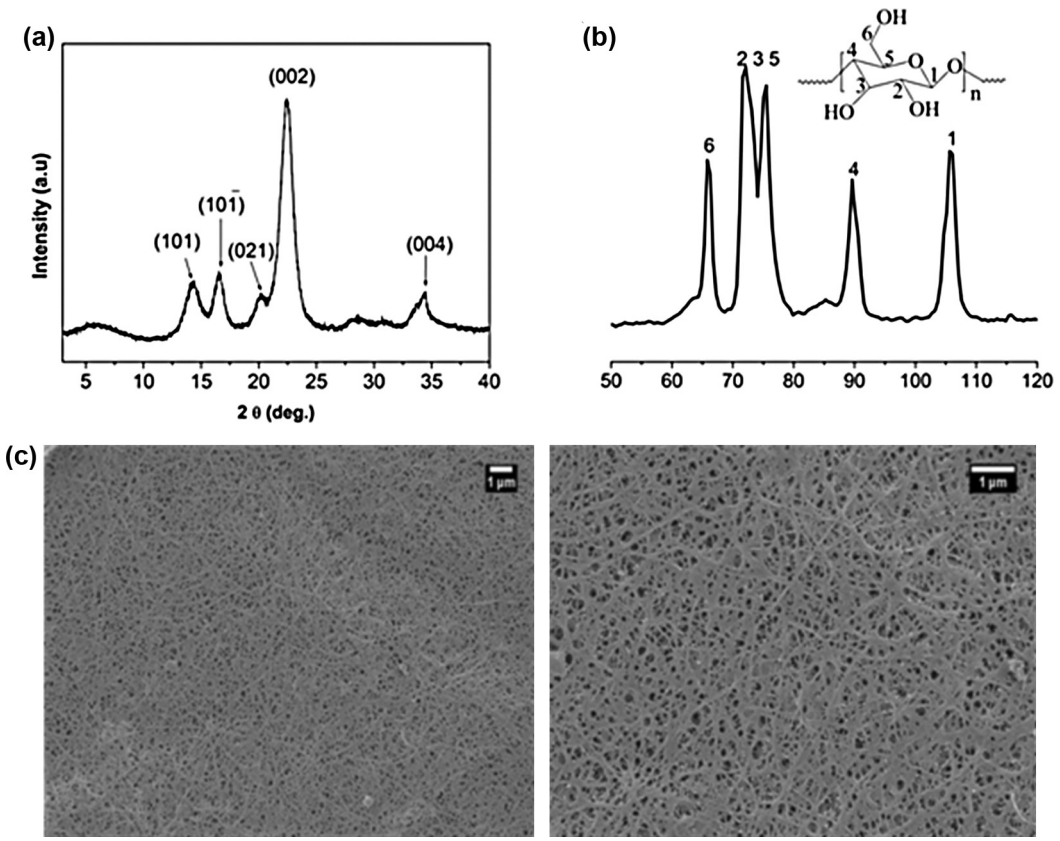

Fig. 1. Characterization of microfibrillated cellulose: (a) XRD pattern, (b) CP/MAS ^{13}C NMR spectrogram, and (c) FE-SEM micrographs of MFC fibers (scale bar 1 μm).

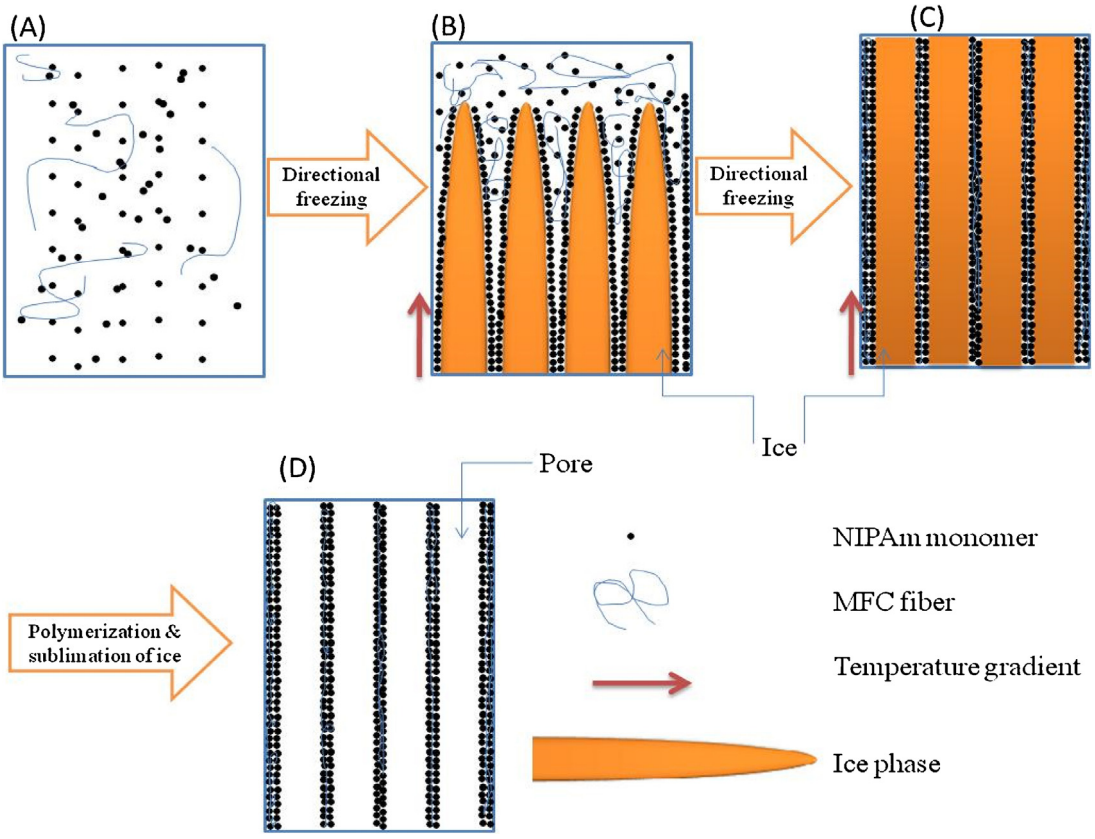

Fig. 2. Preparation route of hydrogels with aligned pores: (A) dispersed MFC fibers in monomer solution, (B) growth of ice crystals following a temperature gradient, (C) polymerization in a directionally frozen state, and (D) after removing the ice phase.

for electron microscopy, swollen hydrogel samples were frozen with liquid nitrogen and then freeze-dried in a freeze-dryer (EYELA FDU 2200, Tokyo, Japan, −86 °C). The surfaces of dried samples were coated with Pt by sputtering for 120 s at 5 V and imaged by a SIGMA/Carl Zeiss (Oberkochen, Germany) electron microscope (5 kV). As a measure of the influence of aligned micropores, water contact angles were measured by using a Phoenix 450 contact angle analyzer (Surface Electro Optics, Gyunggido, Korea). The angles were assessed by using ImageJ software (National Institutes of Health, Bethesda, MD, USA, version 1.46).

The storage and loss moduli of hydrogels 1.5 mm thick and 20 mm in diameter were determined using a CVO Bohlin rheometer (Bohlin Instruments, Cirencester, UK) of parallel plate geometry. The diameter of the upper plate was 20 mm. The experiments were performed using a frequency sweep of 0.1–10 Hz at 25 °C and a constant applied strain of 0.1%.

3. Results and discussion

3.1. Preparation of microfibrillated cellulose

The hydrolysis of cellulosic materials using H_2SO_4 has been widely used to extract cellulose microfibers (Correa et al., 2010; Tischer et al., 2010). The acid hydrolysis preferentially disintegrates disordered or amorphous regions; crystalline domains have a higher resistance to acids and thereby remain intact. The crystallinity, chemical structure, and fibrillar morphology of the MFC prepared as described above was confirmed by XRD, CP/MAS ^{13}C NMR, and FE-SEM (Fig. 1). The characteristic XRD peaks of MFC fibers at 14.5°, 18°, 20°, 22°, and 34.5° respectively corresponded to the crystallographic planes of reflections (1 0 1), (1 0 $\bar{1}$), (0 2 1), (0 0 2), and (0 4 0). These peaks are known for the cellulose I allomorph (Correa et al., 2010; Tischer et al., 2010), and no significant amorphous diffraction can be identified. The CP/MAS ^{13}C NMR spectrum showed relevant peaks in the range of 60–110 ppm, which could be attributed to the cellulose backbones of C-6 (65 ppm); C-2, -3, and -5 (72 ppm); C-4 (89 ppm); and C-1 (105 ppm) (Zuckerstatter, Terinte, Sixta, & Schuster, 2013).

The FE-SEM image in Fig. 1c shows the typical highly entangled and fibrillar morphology of the MFC fibers. The morphology of cellulose fibers depends on their source and on the hydrolysis conditions. While the cellulose nanowhiskers extracted from vegetal resources such as cotton or wood typically have lengths of 100–300 nm and widths of 5–20 nm, nanofibers obtained from tunicin and bacterial cellulose are much longer, with lengths of several micrometers and widths of 5–50 nm (Martínez-Sanz et al., 2011). The characterizations of XRD, CP/MAS ^{13}C NMR, and FE-SEM show that MFC fibers were properly isolated, and were of crystalline structure of the cellulose I allomorph.

3.2. Preparation of PNIPAm and PNIPAm/MFC composite hydrogels

The hydrogels were prepared by directional freezing and *in situ* photopolymerization of NIPAm monomer, MBA crosslinker, and a water-soluble photoinitiator, as shown schematically in Fig. 2. The homogeneous dispersions of MFC and monomer first underwent a directional freezing step, which was triggered by the application of a unidirectional temperature gradient along the thickness direction. Under the temperature gradient, the ice crystallization nucleated at the mold surface closest to the liquid nitrogen reservoir, and crystals grew along the temperature gradient, expelling solutes from the growing ice phase. That is to say, because the solutes usually have very poor solubility in the ice phase, they formed their own cryoconcentrated phases as walls between the growing ice crystals. The freezing rate was determined mainly by the thermal conductivity of the mold and by the gradient, which was known to control the size and morphology of the ice crystals. The directional freezing is a type of controlled melt crystallization, and under the conditions employed herein, a mainly cylindrical crystal morphology was expected to develop (Chung, Lee, & Lee, 2012; Lee, Kim, Chang, & Lee, 2013), so that cylindrical micropores would remain after removing the ice crystals. The porosity can easily be tuned with solute (*i.e.* monomer) concentration. A direct relation between porosity and the concentration of initial solution (or dispersion) was previously reported: The cellulose microfibrillar foams prepared with various concentrations of MFC suspension (2.0 up to 8.0 wt%) have porosities from 98.7% to 94.7% (Lee et al., 2000).

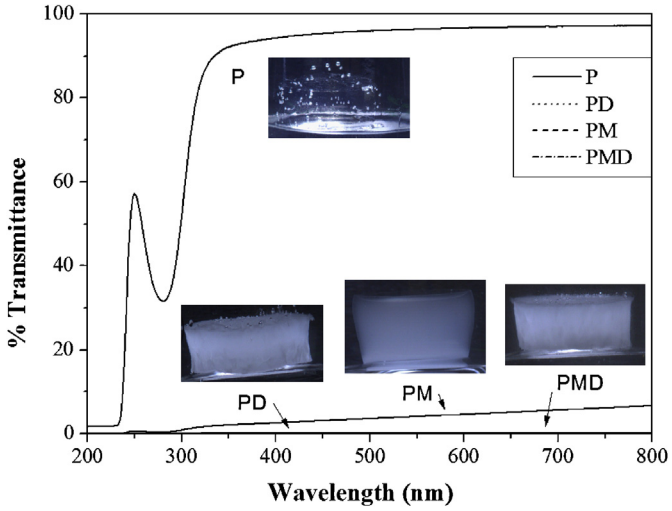

Fig. 3. UV–vis absorbance and transparency of four hydrogels, with corresponding images.

PNIPAm hydrogels are typically synthesized by a free radical polymerization in an aqueous medium using a free radical initiator such as a UV, redox, or thermal initiator; for these syntheses, the use of an inert environment, a proper temperature, and a proper reaction time are important. Herein, UV photopolymerization was utilized to retain the directionally frozen structures as well as possible. Heat from the UV illumination can destroy the developed internal structures, but this heat can also enable effective crosslinking by melting the precursors; therefore, a proper balance is necessary between the melting rate and the UV-induced polymerization rate. Beginning from the top surface facing a UV lamp, the photon energy starts to melt the ice crystal phase. Then, the UV-responsive initiator decomposes and produces highly reactive free radicals, causing polymerization to propagate rapidly. During the propagation of PNIPAm chains, MFC fibers become embedded within the three-dimensional hydrogel networks (Fig. 2B and C).

The UV polymerization conditions were developed by varying the illumination time from 30 min to 1 h and investigating the morphology of the resulting hydrogels. In our early development work, pure PNIPAm hydrogels were successfully crosslinked within 30 min. However, the presence of either MFC or directional micropores increased the required crosslinking time. This is possibly due to UV light scattering at the surfaces of the MFC or at the interfaces between the ice phases and cryoconcentrates. Moreover, the mere presence of embedded MFC fibers and aligned ice crystals could hinder UV penetration, initiator decomposition, and propagation of active radicals.

Fig. 3 shows the UV–vis transmittance of hydrogels and their corresponding optical images. The near 100% transmittance of P in the wavelength range of 350–800 nm is indicative of a

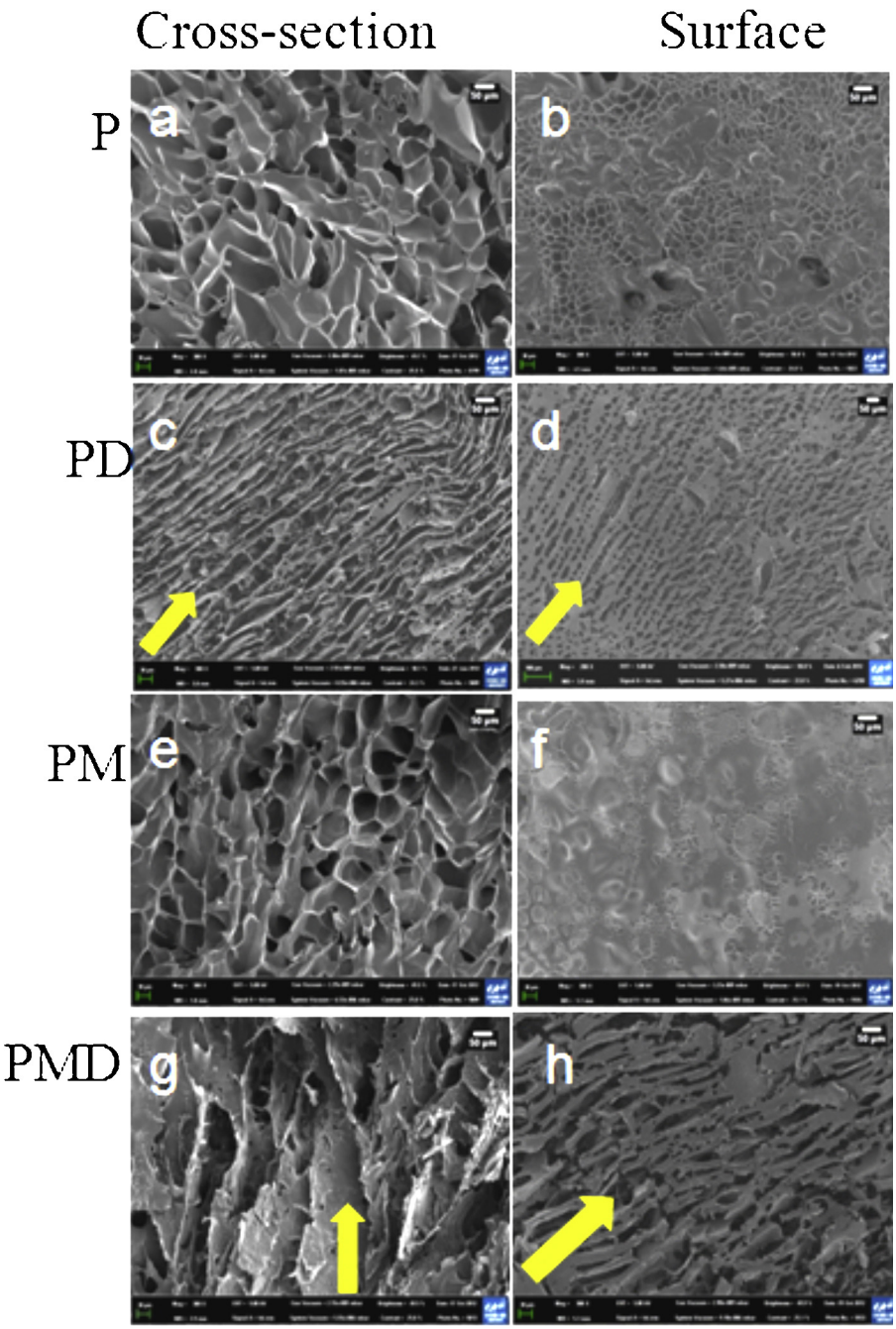

Fig. 4. Cross-sectional and surface morphologies, respectively, of (a, b) P; (c, d) PD; (e, f) PM; and (g, h) PMD. Scale bars are 50 μm. Arrows indicate the direction of ice crystal growth.

homogeneous gel network structure free from any inhomogeneities on the micrometer or sub-nanometer scale, such as micropores. The presence of micropores, fibers, or both made PD, PM, and PMD UV–vis opaque; this finding is clearly supported by the sample images in Fig. 3. Among the 3 opaque samples, PM is the most transparent, indicating the smaller dimensions of the MFC relative to the aligned pores. Embedded micropores and fibers have different refractive indexes, causing significant light scattering at their interfaces, particularly micropores.

The transparency of P depended on its preparation temperature. It is well known that the preparation temperature of PNIPAm impacts its chemical and physical properties by changing the homogeneity of its network; namely, if the preparation temperature is below the LCST, a homogeneous and transparent hydrogel is formed, but above the LCST, a morphologically heterogeneous and opaque hydrogel is formed (Hou et al., 2008). The mechanical properties also vary with preparation temperature. Our spectroscopic results (Fig. 3) are consistent with those of previous studies (Hou et al., 2008).

3.3. Micropore morphologies

To prepare samples for SEM investigation, they were freeze-dried; however, to preserve the natural morphologies of their swollen states, they were first flash-frozen in liquid nitrogen. This sample preparation was able to reveal the effects of the directional freezing on the resulting morphology (Fig. 4), although with a certain degree of damage related to cryo-stress or desiccant stress. The

porous structures in P were typical of the freeze-dried hydrogels, and their presence indicated the networked structure and intrinsic inhomogeneity of PNIPAm. The pores corresponded to the shape of the ice crystal phases, since the ice crystals were removed under vacuum during freeze-drying, leaving these pores behind. The ice crystals in P and PM seemed to have formed quite randomly under the influences of the PNIPAm structures, resulting in almost closed pore structures.

Aligned micropores were noticeable in the cases of PD and PMD but not in the cases of P and PM, clearly showing that the directional freezing caused this alignment (Fig. 4). These micropores were aligned along the temperature gradient (Barrow & Zhang, 2013; Chen et al., 2012). Both cross-sections and surfaces show aligned micropores; the pores appear to slightly vary in morphology between cylindrical and lamellar forms of 50–100 μm, but are mainly cylindrical. The cross-sectional images show the alignment of micropores along the main temperature gradient from the liquid nitrogen reservoir (Fig. 4c and g). Although the main temperature gradient was imposed perpendicularly to the sample surface, there were also slight differences in thermal diffusion, causing a weak but noticeable in-plane temperature gradient on the surface. The surface alignments (Fig. 4d and h) can be attributed to these in-plane temperature gradients.

Cooling by a liquid nitrogen reservoir provided local supercooling states in monomer solution. Once the degree of supercooling (or freezing rate) reached a certain degree, Mullins-Sekerka instability occurred, creating ice crystals of cellular (micropore-like) or dendrite (ladder-like) structure (Lee & Deng, 2011; Qian & Zhang, 2011). Similar morphologies were reported in previous studies on poly(2-hydroxyethyl methacrylate) hydrogels, which proved the possibility of fabricating anisotropic hydrogels using the directional freezing technique (Chen et al., 2012).

In the process of unidirectional freezing, NIPAm, MBA, initiator, and MFC were expelled from the ice crystal phases, and the subsequent illumination of UV light triggered *in situ* polymerization and immobilized the MFC fibers. Probably, MFC experiences different exclusion forces than other small molecules, owing to its different size and surface energy. But no accumulated MFC phases were noticed in our SEM investigation; the MFC seemed to be homogeneously embedded in the PNIPAm networks with aligned micropores.

In all the different sample types, micropores on the surface were smaller than the internal micropores seen in cross-sections. This result is qualitatively consistent with previous investigations; fast freezing is known to produce smaller ice crystals (Kim, Lee, & Lee, 2013). Under the assumptions of Fickean diffusion, Rohatgi and Adams proposed the following relation between ice crystal size (L) and freezing rate (F): $L \sim F^{-0.5}$. In our previous studies on the directional freezing of polymer solutions, this relation was applicable qualitatively, but not quantitatively.

3.4. Swelling characteristics

The temperature dependence of SR of hydrogels in distilled water (Fig. 5) showed a general switch from relatively large swelling to deswelling at around 32 °C, corresponding to the LCST of PNIPAm. It is apparent that the phase transition temperature was unaffected by the embedded MFC fibers or the aligned micropores prepared by unidirectional freezing. However, the swelling ratio changes (volume changes) upon this transition did differ among the different hydrogels. PD, PM, and PMD all had larger volume changes than P. Therefore, both the incorporation of MFC and the introduction of aligned micropores made the volume transition more distinct. In typical hydrogels, an increase in volume change is generally followed by a decrease in crosslink density and modulus.

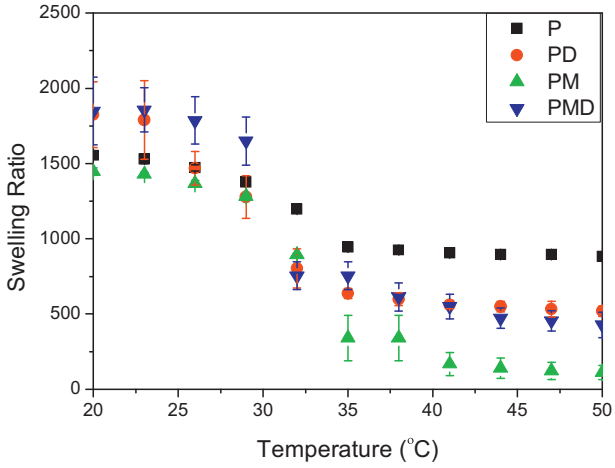

Fig. 5. Swelling ratio of hydrogels as a function of temperature.

Herein, the volume change was able to be engineered without modifying the crosslink density.

The differences in volume change can be analyzed by comparing swelling ratios and also swelling/deswelling kinetics below and above the LCST. The Flory–Rehner theory describes that the swelling process of hydrogels is based on three terms including mixing, elastic and ionic terms (Zhao, Li, Xia, Bajalis, & Xi, 2008). The present work consists of non-polyelectrolyte hydrogels in distilled water. Therefore, the elastic and mixing driving forces were the parameters that control the swelling rate. In addition, the aligned micropores can make the diffusion of water molecules faster during the swelling/deswelling process. Particularly, anisometric swelling behavior can be expected.

PNIPAm (P) is known to exist in an uncoiled state below its phase transition temperature. P showed a relatively large equilibrium swelling of 1550% (Fig. 5), mainly due to hydrogen bonding interactions between its amide groups and water. By contrast, unidirectionally frozen PD swelled more, up to *ca.* 1800%; PM swelled 1440% and PMD swelled 1850%. The higher SRs of PD and PMD can be explained by the microporous structures created by directional freezing. These micropores could increase the free volume of hydrogel available for water molecules. On the other hand, the presence of MFC does not significantly change the SR below the LCST, despite the fact that cellulose fibers exhibit a strong hydrogen bonding tendency.

Cellulose fibers are known to exhibit strong hydrogen bonding with adjacent cellulose microfibrils as well as PNIPAm chains. Above the LCST, PNIPAm chains start to adopt a coiled conformation, expelling surrounding water molecules. The existence of MFC seems to promote this collapsing process further, judging by the much smaller SR of PM above the LCST, compared to that of P (Fig. 5). Strong hydrogen bonding between PNIPAm and MFC is expected to develop concurrently. The existence of micropores also allowed more shrinking above the LCST. The increased free volume of the hydrogels seemed to help the large volume shrinking process. Large volume shrinking always entails the development of internal misfit stress, and the presence of micropores will release the misfit stress to a certain degree. These mechanisms related to equilibrium swelling explain the increased volume changes of PD, PM, and PMD relative to P.

Fig. 6 shows the dynamic water swelling behavior of hydrogels at the initial penetration stages. Water droplets on the surfaces of freeze-dried hydrogel samples were monitored over time right after each water droplet contacted the surface. The presence of aligned micropores in the hydrogels decreased the contact angle at a given time after contact; initially, all the hydrogels showed

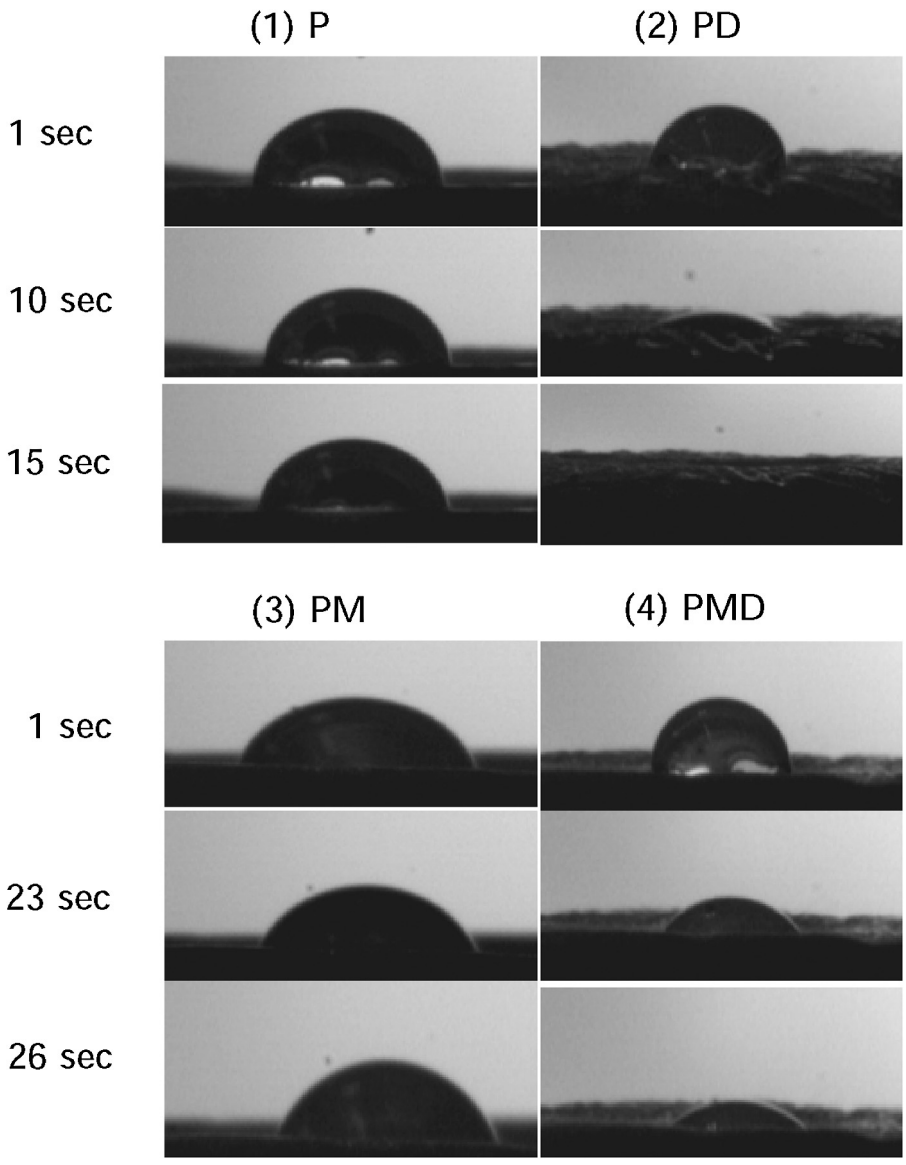

Fig. 6. Contact angle measurements of hydrogels at various times after a water drop touches the sample surface.

a contact angle of about 90°, but in the cases of PD and PMD, the contact angle decreased to zero rapidly. For example, after 15 s, the contact angle P had decreased slightly to 85°, whereas the contact angle of PD had reached zero as the water drop was completely absorbed. Similarly, PM shows an initial contact angle of 88°, and 66° and 63° angles after 23 and 26 s, respectively, while PMD showed relatively fast absorption.

The faster reduction of contact angle is caused by rapid water absorption through the vertically aligned porous structures. These aligned micropores allow water to be absorbed quickly into the dried matrix due to the capillary force of the open micropores. As a result, the introduction of aligned micropores by directional freezing not only increases equilibrium swelling but also increases the water absorption rate; that is, the speed of swelling. These are the desired properties for superporous hydrogels. Similarly, because the aligned open micropores act as diffusion channels, fast deswelling is also expected.

3.5. Rheological properties

When shear strain is applied to a swollen hydrogel, the ratio of resulting in-phase stress to strain (γ) represents the elastic component, called the storage (or elastic) modulus (G'), and the ratio of out-of-phase stress to strain represents the viscous components, called the loss modulus (G'') (Jahromi, Grover, Paxton, & Smith Alan, 2011). General features observed for all the hydrogels are a pronounced plateau of G' in the full frequency range with weak shear thickening behavior and $G' > G''$; these all indicate the formation of gels (Harini and Deshpande, 2009; Jahromi et al., 2011; Wang et al., 2012).

The comparison of the hydrogels P, PD, PM, and PMD revealed that the elastic modulus (G') increased with MFC loading and decreased with the introduction of micropores by directional freezing (Fig. 7). This suggests that MFC in the form of aligned macromolecular chains plays an important role in improving deformation resistance, as was expected based on its unique crystalline structure and strong hydrogen bonding. Entanglement between MFC fibers, which can be discerned in Fig. 1, might be essential in strengthening the hydrogels. The possible interactions between MFC and PNIPAm *via* hydrogen bonding will further assist the load transfer from the matrix into the fibers, which could allow the MFC to contribute to stiffening. A possible reason for the decrease in modulus by the introduction of micropores is an increase in SR (*i.e.*, higher porosity) (Fig. 5). The lower chain density of hydrogels

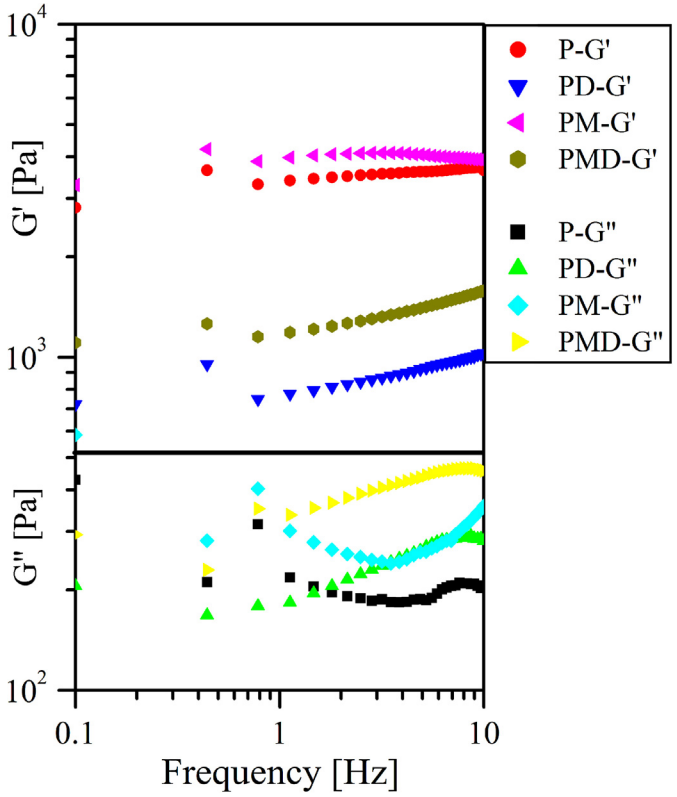

Fig. 7. Viscous and elastic moduli of hydrogels at 25 °C as a function of frequency.

with increased SR means that they are inevitably mechanically weaker.

4. Discussion

The rubber elasticity theory of random Gaussian networks provides the following relation between G' and swelling ratio (SR):

$$G' = \frac{cRT}{Mc},$$

where c is polymer concentration (g/m^3, SR = $\rho/c - 1$, where ρ is density of hydrogel), and M_c is the molecular weight between crosslinks (g) (Kuen, Jon, Petra, & Erick, 2000). If this simple freely jointed chain model were valid in our systems, the ratio G'/c should be constant for the four hydrogels because they were crosslinked in the same condition. However, the ratios measured from Figs. 5 and 7 varied from 1.4 to 5.0 Nm/g, using the density of water at 25 °C. Although G' generally increases with an increase in c, the observed variation was quite significant. Above the LCST, the swelling ratios may deviate even more significantly from the rubber elasticity theory. PD and PMD have higher SRs than P below the LCST, but above the LCST, they showed the reverse behavior, with lower SRs than P. Thus, more variation of G'/c ratio may be anticipated. The temperature dependence of SR has usually been explained by the temperature dependence of the interaction parameter (Hou et al., 2008). That explanation is not quite applicable herein, since the same PNIPAm network was used for all the four hydrogels, and thus the interaction parameter was the same.

The greater deviation from the rubber elasticity theory seems to originate from the nanoscale and microscale structures, rather than from the molecular chain structures that are the focus of the rubber elasticity theory. The nanoscale MFC structures brought about a significantly lowered SR above the LCST, possibly because of their interaction with the PNIPAm networks. The microscale pores brought about rapid water infiltration behavior, and also induced a decrease in SR above the LCST. These properties are outside what the rubber elasticity theory can explain; they can instead be explained by specific interactions, internal misfit stress developed during hydrogel deswelling, free volume of pores, fiber entanglement, *etc.*, as discussed above. Recently, the misfit stress that develops inside hydrogels was reported to play an important role in determining their swelling properties (Lee et al., 2013).

The *in situ* photopolymerization method successfully immobilized aligned micropores inside hydrogels. During the UV polymerization in a frozen state, polymerization occurs at subzero temperature, without the macromolecular chain breakage that would occur during freezing if the polymerization were carried out first. It was recently reported that hydrogels prepared by directional freezing and redox polymerization had anisotropic microstructures including regularly aligned long channels of 20–50 μm (Convertine et al., 2006).

In summary, the introduction of aligned micropores can significantly increase the SR below the LCST and can increase the amount of volume change. Furthermore, the micropores allow fast water infiltration, another advantage for superporous hydrogels. The use of micropores inevitably deteriorates the modulus, but this can be compensated for by including MFC as a reinforcing material.

5. Conclusions

To widen the applicability of temperature-responsive hydrogels, nanostructures and microstructures were introduced together into a PNIPAm matrix. MFC fibers purified from bacterial cellulose were used as the nanostructures, and aligned micropores fabricated by directional freezing were used as microstructures. The directional freezing was carried out following a temperature gradient, successfully triggering the nucleation and growth of cylindrical ice phases. While retaining the MFC/monomer/ice structures, *in situ* UV photopolymerization permanently immobilized the dispersed MFC fibers and the aligned micropores into PNIPAm networks. The aligned micropores corresponded to the space of the cylindrical ice phases; these pores enabled rapid water infiltration and increased the volume changes upon the LCST transition. The use of MFC also increased the volume changes and elastic shear modulus. These properties are outside what the typical molecular chain architecting can offer, and the composite hydrogels are potentially applicable to a wide range of emerging areas such as thermoresponsive superabsorbents and microporous scaffolds.

Acknowledgements

This work was supported by the National Research Foundation grant funded by the Korea Ministry of Science, ICT & Future Planning (NRF-2012R1A2A2A01014107 & NRF-2013R1A1A2021573), and a grant from the Korea Healthcare Technology R&D Project, Ministry of Health & Welfare, Republic of Korea (No. A103017).

References

Bajpai, A. K., Shukla, S. K., Bhanu, S., & Kankane, S. (2008). Responsive polymers in controlled drug delivery. *Progress in Polymer Science*, *33*, 1088–1118.

Barrow, M., & Zhang, H. (2013). Aligned porous stimuli-responsive hydrogels via directional freezing and frozen UV initiated polymerization. *Soft Matter*, *9*, 2723.

Bhattacharyya, S., Guillot, S., Dabboue, H., Tranchant, J., & Salvetat, J. (2008). Carbon nanotubes as structural nanofibers for hyaluronic acid hydrogel scaffolds. *Biomacromolecules*, *9*, 505–509.

Breedveld, V., Nowak, A. P., Sato, J., Deming, T. J., & Pine, D. J. (2004). Rheology of block copolypeptide solutions: Hydrogels with tunable properties. *Macromolecules*, *37*, 3943–3953.

Chen, M., Zhu, J., Qi, G., He, C., & Wang, H. (2012). Anisotropic hydrogels fabricated with directional freezing and radiation-induced polymerization and crosslinking method. *Materials Letters*, *89*, 104–107.

Chen, W., Yu, H., Liu, Y., Chen, P., Zhang, M., & Hai, Y. (2011). Individualization of cellulose nanofibers from wood using high-intensity ultrasonication combined with chemical pretreatments. *Carbohydrate Polymers*, *83*, 1804–1811.

Cho, E. C., Lee, J., & Cho, K. (2003). Role of bound water and hydrophobic interaction in phase transition of poly(N-isopropylacrylamide) aqueous solution. *Macromolecules*, *36*, 9929–9934.

Chung, N., Lee, M., & Lee, J. (2012). Mechanism of freeze-drying drug nanosuspensions. *International Journal of Pharmaceutics*, *437*, 42–50.

Convertine, A. J., Lokitz, B., Vasileva, S., Myrick, V., Scales, L. J., Lowe, C. W., et al. (2006). Direct synthesis of thermally responsive DMA/NIPAM diblock and DMA/NIPAM/DMA triblock copolymers via aqueous, room temperature RAFT polymerization. *Macromolecules*, *39*, 1724–1730.

Correa, A. C., Teixeira, E. M., Pessan, L. A., & Mattoso, L. H. C. (2010). Cellulose nanofibers from curaua fibers. *Cellulose*, *17*, 1183–1192.

Gong, J. P., Katsuyama, Y., Kurokawa, T., & Osada, Y. (2003). Double-network hydrogels with extremely high mechanical strength. *Advanced Materials*, *15*(14), 1155–1158.

Harini, M., & Deshpande, A. P. (2009). Rheology of poly(sodium acrylate) hydrogels during cross-linking with and without cellulose microfibrils. *Journal of Rheology*, *53*(1), 1–47.

Hou, Y., Matthews, A. R., Smitherman, A. M., Bulick, A. S., Hahn, M. S., Hou, H., et al. (2008). Thermoresponsive nanocomposite hydrogels with cell-releasing behavior. *Biomaterials*, *29*, 3175–3184.

JagadeeshBabu, P. E., Suresh Kumar, R., & Maheswari, B. (2011). Synthesis and characterization of temperature sensitive P-NIPAM macro/micro hydrogels. *Colloids and Surfaces A: Physicochemical and Engineering Aspects*, *384*, 466–472.

Jahromi, S. H., Grover, L. M., Paxton, J. Z., & Smith Alan, M. (2011). Degradation of polysaccharide hydrogels seeded with bone marrow stromal cells. *Journal of Mechanical Behavior of Biomedical Materials*, *4*, 1157–1166.

Kim, B., Lee, Mi., & Lee, J. (2013). Large-area PVDF membranes with through-thickness porosity prepared by uni-directional freezing. *Macromolecular Research*, *21*(2), 194–201.

Kuen, Y. L., Jon, A. R., Petra, E., Erick, M. M., Kamal, H. B., & David, J. M. (2000). Controlling mechanical and swelling properties of alginate hydrogels independently by cross-linker type and cross-linking density. *Macromolecules*, *33*, 4291–4294.

Lazarides, E. (1976). Actin, α-actinin, and tropomyosin interaction in the structural organization of actin filaments in nonmuscle cells. *Journal of Cell Biology*, *68*, 202–219.

Lee, J., & Deng, Y. (2011). The morphology and mechanical properties of layer structured cellulose microfibril foams from ice-templating methods. *Soft Matter*, *7*, 6034–6040.

Lee, K., Rowley, J. A., Rowley, J. A., Eiselt, P., Moy, E. M., Bouhadir, K. H., et al. (2000). Controlling mechanical and swelling properties of alginate hydrogels independently by cross-linker type and cross-linking density. *Macromolecules*, *33*(11), 4291–4294.

Lee, M., & Lee, J. (2013). Fabrication of ferroelectric polymer nanocrystals with tunable morphologies. *Crystal Growth & Design*, *13*, 671–678.

Lee, S., Kim, H., Chang, S., & Lee, J. (2013). Anisometric nanocomposite hydrogels with temperature responsive compartments. *Soft Matter*, *9*, 472.

Li, G., Guo, L., Chang, X., & Yang, M. (2012). Thermo-sensitive chitosan based semi-IPN hydrogels for high and loading and sustained release of anionic drugs. *International Journal of Biological Macromolecules*, *50*, 899–904.

Martínez-Sanz, M., Lopez-Rubio, A., & Lagaron, J. M. (2011). Optimization of the nanofabrication by acid hydrolysis of bacterial cellulose nanowhiskers. *Carbohydrate Polymers*, *85*, 228–236.

Nishihara, H., Mukai, S. R., Fujii, Y., Tago, T., Masudac, T., & Tamon, H. (2006). Preparation of monolithic SiO_2–Al_2O_3 cryogels with inter-connected macropores through ice templating. *Journal of Materials Chemistry*, *16*, 3231–3236.

Qian, L., & Zhang, H. (2011). Controlled freezing and freeze drying: A versatile route for porous and micro-/nano-structured materials. *Journal of Chemical Technology and Biotechnology*, *86*, 172–184.

Singh, D., Kuckling, D., Choudhary, V., Adler, H., & Koul, V. (2006). Synthesis and characterization of poly(N-isopropylacrylamide) films by photopolymerization. *Polymers for Advanced Technologies*, *17*, 186–192.

Tischer, P. C. S. F., Sierakowski, M. R., Jr., & Tischer, H. W. C. A. (2010). Nanostructural reorganization of bacterial cellulose by ultrasonic treatment. *Biomacromolecules*, *11*, 1217–1224.

Wang, T., Liu, D., Lian, C., Zheng, S., Xinxing, L., & Tong, Z. (2012). Large deformation behavior and effective network chain density of swollen poly(N-isopropylacrylamide) – laponite nanocomposite hydrogels. *Soft Matter*, *8*, 774–783.

Xia, X., Yih, J., D'Souza, N. A., & Hu, Z. (2003). Swelling and mechanical behavior of poly(N-isopropylacrylamide)/namontmorillonite layered silicates composite gels. *Polymer*, *44*, 3389–3393.

Yildirim, D. E., Yin, X., Nair, K., & Sun, W. (2008). Fabrication, characterization, and biocompatibility of single-walled carbon nanotube-reinforced alginate composite scaffolds manufactured using freeform fabrication technique. *Journal of Biomedical Materials Research Part B: Applied Biomaterials*, *87B*, 406–414.

Zhao, Z. X., Li, Z., Xia, Q., Bajalis, Q. B., & Xi, H. X. (2008). Swelling/deswelling kinetics of PNIPAAm hydrogels synthesized by microwave irradiation. *Chemical Engineering Journal*, *142*, 263–270.

Zhou, C., & Wu, Q. (2011). A novel polyacrylamide nanocomposite hydrogel reinforced with natural chitosan nanofibers. *Colloids and Surfaces B: Biointerfaces*, *84*, 155–162.

Zuckerstatter, G., Terinte, N., Sixta, H., & Schuster, K. C. (2013). Novel insight into cellulose supramolecular structure through 13C CP-MAS NMR spectroscopy and paramagnetic relaxation enhancement cellulose solid state NMR. *Carbohydrate Polymers*, *93*, 122–128.